Nanoscale Advances

ROYAL SOCIETY OF CHEMISTRY

PAPER

View Article Online
View Journal | View Issue

Cite this: *Nanoscale Adv.*, 2024, **6**, 534

An ALP enzyme-based electrochemical biosensor coated with signal-amplifying $BaTiO_3$ nanoparticles for the detection of an antiviral drug in human blood serum†

Muhammad Umar Draz,[a] Muhammad Zia Ul Haq,[a] Akhtar Hayat *[b] and Huma Ajab *[c]

Tenofovir (TFV) is an antiviral drug used to treat the co-infections of HIV/HBV viruses. Accurate monitoring of TFV drug levels is essential for evaluating patient adherence, optimizing dosage, and assessing treatment efficacy. Herein, we propose an innovative electrochemical sensing approach by using the alkaline phosphatase (ALP) enzyme with the support of $BaTiO_3$ nanoparticles. An attractive sensitivity and selectivity of the developed sensor towards TFV detection were achieved. First, the nanoparticles were synthesized by following a single-step sol–gel method and characterized through various analytical techniques, including SEM, EDX, FT-IR, BET, zeta potential, XRD, and UV-vis and Raman spectroscopy. The suggested mechanism demonstrated the formation of a strong bond between TFV and the ALP enzyme, primarily through the phosphate group, resulting in enzyme inhibition. Various parameters like nanoparticle amount, electrode modification time with enzyme and $BaTiO_3$ nanoparticles, and drug incubation time were optimized. The biosensor demonstrated an outstanding limit of detection (LOD) of 0.09 nM and recovery percentages of 98.6–106% in human blood serum, indicating adequate repeatability and selectivity. The proposed biosensor can be converted into a portable device for measuring small sample volumes and observing patients for immediate medical care or personalized therapies. It achieved better sensitivity compared to existing methods, making it suitable for precise drug detection in microdoses.

Received 29th September 2023
Accepted 29th November 2023

DOI: 10.1039/d3na00839h

rsc.li/nanoscale-advances

1. Introduction

The two most lethal and rapidly spreading fatal diseases in the world are hepatitis B (HBV) and human immunodeficiency syndrome (HIV). Due to the presence of reverse transcriptase enzymes, both viral infections may have a substantial impact on human health. In particular, a precarious form of the hepatitis B virus, known as HBV, can severely damage liver tissues,[1,2] leading to over 800 000 deaths worldwide.[3] In the same way, HIV, the virus that causes acquired immunodeficiency syndrome (AIDS), eliminates CD4 T-cells, impairing immunity and making the body susceptible to other infections.[4] Every year, at least 5000 people die from AIDS.[5] In developing countries, like Pakistan, HIV infections have surged by 17.6%, significantly exceeding the global rate of 2.2%. This increase is primarily due to factors such as overseas work, low awareness, stigma, unsafe practices, and limited healthcare access.[6]

The rapid spread of infectious diseases like HIV/AIDS is primarily driven by sexual contact (52.55%), infected people's blood (11.73%), and needle-sharing,[6,7] posing a global threat.[8] To reduce transmission rates and ensure survival, a range of services are needed, including diagnosis, medical care, and preventive measures. Significant success has been made in preventing this co-infection by utilizing over 20 different antiviral drugs in various nations, despite the HIV epidemic's dramatic rise over the past ten years.[9]

Of these drugs, TFV is one of the most successful regimens administered for HIV/HBV illnesses; nevertheless, it is also associated with several major health risks, including damage to the kidneys, liver, stomach, and bones. Therefore, it is essential to precisely track the patients' levels of the drug TFV in order to ensure appropriate dosing, prevent drug resistance, evaluate efficacy, assess treatment effectiveness, and verify patient observance.[10]

[a]*Department of Chemistry, COMSATS University Islamabad, Abbottabad Campus, Pakistan. E-mail: umar.comsatsatd@gmail.com; muhammad.umar115@amalacademy.org; zia.comsatsatd@gmail.com; ziaulhaqm893@gmail.com*

[b]*Interdisciplinary Research Centre in Biomedical Materials (IRCBM), COMSATS University, Islamabad Lahore Campus, Lahore 54000, Pakistan. E-mail: akhtarhayat@cuilahore.edu.pk*

[c]*Department of Chemistry, COMSATS University Islamabad, Abbottabad Campus, Abbottabad, Pakistan. E-mail: humaajab@cuiatd.edu.pk*

† Electronic supplementary information (ESI) available. See DOI: https://doi.org/10.1039/d3na00839h

TFV, referred to by its chemical name [(2*R*)-1-(6-aminopurine-9-yl) propane-2-yl] oxymethylphosphonic acid, is a nucleotide analog reverse transcriptase inhibitor that is used to treat fatal HIV/AIDS and HBV infections. It was first developed by Gilead and authorized by the US Food and Drug Administration (FDA). The mechanism of action of TFV in patients with HIV and HBV involves the restriction of viral reverse transcriptase enzyme activity and termination of DNA replication through competing with deoxyadenosine 5′-triphosphate.[11–13] Thus, it is quite desirable to investigate and develop an efficient method for rapidly determining the targeted drug.

Various analytical methods, such as nuclear magnetic resonance (NMR), thin-layer chromatography (TLC), liquid chromatography coupled with mass spectrometry (LC-MS), infrared spectroscopy (IRS), high-performance liquid chromatography (HPLC), and spectrophotometry, have been validated by researchers, physicians, quality analysts, and regulatory agencies to be accurate in measuring and identifying TFV.[14,15] Despite their selectivity and reliability, these techniques have a number of serious disadvantages, such as high costs, labor-intensive manual processes, costly equipment requirements, and protracted handling procedures with multiple steps.[16]

Unlike the approaches discussed earlier, electrochemical sensors have garnered considerable attention in healthcare and point-of-care diagnostic applications.[17] These advantages include excellent mobility, high sensitivity, quick response, affordability, reliability, low background current, simplicity in handling, and automation.[18,19] However, due to the presence of proteins,[21] electrochemical techniques may face difficulties such as electrode fouling, which hinders electron transport,[20] and causes interference when analyzing real samples for free drug (pharmacologically active) concentrations.[21]

Unmodified electrodes have a few drawbacks in electrochemical sensing, including slower electron transfer kinetics, reduced reproducibility, and sensitivity at high potentials.[22] Researchers are working on electrode modification using active materials such as enzymes, aptamers, and nanomaterials such as titanates and metal oxides to improve selectivity and sensitivity.[23]

Nanomaterial based modifications are gaining popularity due to their unique characteristics such as fast electron transfer, nanosize, stability, energy efficiency, and catalytic performance.[24] Some studies have explored the electrochemical detection of TFV drugs using nanomaterials: Xiao *et al.* reported ZrO_2-CS-MWCNTs/GCE,[2] Mehmandoust *et al.* reported MIP-PT@g-C_3N_4/F-MWCNT,[9] Alake *et al.* developed an electrode with NiS@PAA-MWCNT,[13] Zeng *et al.* used La_2O_3–ZrO_2-MWCNTs/GCE,[11] Festinger *et al.* proposed GO/GCE and Hg(Ag)FE,[25] and Ozcelikay *et al.* utilized benzalkonium chloride/AgNPs.[26] It is imperative to conduct a thorough assessment in order to obtain accurate and timely detection of the TFV drug with a cost-effective and feasible implementation.

$BaTiO_3$ nanoparticles, a well-known metal oxide, are currently attracting attention because of their exceptional stability and scavenging capabilities. $BaTiO_3$, a member of the ABO_3 perovskite family, has an octahedrally coordinated unit cell with Ba^{2+} and Ti^{4+} ions forming a network of oxygen atoms.[27] $BaTiO_3$ nanoparticles are particularly regarded as promising in the field of biosensing due to their unique attributes like biocompatibility,[28] catalysis,[29] piezoelectric effect,[30] second harmonic generation, and low dielectric constant.[31] ALP, an inexpensive enzyme with active ions at its center, assisted in attachment *via* a variety of bonding forces to the $BaTiO_3$ modified electrode.[32] Because of its affordability and rapid turnover, ALP is frequently used in immunological, gene, and aptamer-based assays, histochemical staining, and similar affinity techniques for monitoring nucleic acids, proteins, enzymes, medications, and other analytes.[17]

This study uses electrochemical and UV-visible spectroscopy techniques to investigate the unique catalytic activity of $BaTiO_3$ nanoparticles for TFV detection. The enzyme alkaline phosphatase (ALP) was used to convert P-nitrophenyl phosphate (PNPP) to P-nitrophenol (PNP). A high voltage is necessary for PNPP to oxidize the analyte quickly electrochemically. However, PNPP has low sensitivity and stability, and $BaTiO_3$'s use in biosensor design improved the sensing platform's performance. $BaTiO_3$ nanoparticles enhance sensitivity and detection limits in electrochemical ALP detection by enhancing product oxidation and amplifying electrochemical signals for ALP-catalyzed products. $BaTiO_3$ nanoparticles were utilized to regulate an enzyme's activity and protect it from potential environmental changes that could lead to rapid denaturalization. This novel application addresses challenges (interferences) in detecting the TFV drug in complex blood samples with proteins and molecules.

When drug concentrations in blood or plasma are low due to microdoses, it becomes difficult to detect drugs precisely. Consequently, sensitive detection techniques are required for precise measurement. A single-step sol–gel approach was used to synthesize $BaTiO_3$ nanoparticles, reducing time-consuming processes and utilizing pencil graphite electrodes (PGEs) as a transducer platform. Because graphite contains sp^2 hybridized carbon atoms with delocalized π electrons, a PGE is widely used in electrochemistry for a number of applications. When considering alternatives like glassy carbon electrodes, using a PGE as the working electrode has a number of advantages over other options, including availability, conductivity, surface modifiability for each trial, and cost and time savings.

After synthesis, the $BaTiO_3$ nanomaterials were characterized using various analytical techniques, including UV-vis spectroscopy, FT-IR, BET, zeta potential, SEM, EDX, XRD, and Raman analysis. Critical parameters, including material concentration, electrode modification time with nanoparticles, and the impact of nanoparticles on enzyme activity, were systematically optimized. The sensitivity and selectivity of the sensor were evaluated in more detail. The method was tested for reproducibility and used on real-medium samples (blood serum). Furthermore, phenol and the substrate PNPP were used to verify the efficacy of the developed method through the use of cyclic voltammetry (CV) and UV-visible spectroscopy techniques.

2. Experimental section

Scheme 1 depicts the proposed $BaTiO_3$/ALP/TFV/PGE sensor. (a) An economical and simple sol–gel method was used for the

synthesis of $BaTiO_3$ nanoparticles; (b) in the second step, the ALP enzyme and the signal-amplifying $BaTiO_3$ nanoparticles were modified over the PGE; (c) the final stage demonstrated a potential mechanism for the detection of the TFV drug by using a fabricated electrode with 2D and 3D structures.

2.1. Apparatus/software

A potentiostat (AMEL, models 2553 and 2700) with three electrode systems, *i.e.*, a reference electrode (Ag/AgCl, 1 M saturated KCl), a platinum counter electrode, and high-quality pencil graphite, acting as a working electrode (WE) was employed to conduct the electrochemical tests. All three electrodes were properly washed by using double-distilled water (DDW) before each and every experiment. A digital pH meter (STARTER 3100, OHAUS) was used to adjust the desired pH of the solution. K. Roy's smart electronic balance (model number 108) and Abron Exports' magnetic stirrer hot plate (model number MSWHP) were used for weighing and stirring, respectively, during the synthesis of $BaTiO_3$ nanoparticles. For the characterization study, the following techniques were used: UV-visible (Specord 200+ of Analytik Jena's, serial no. 223E2003C, Germany), Fourier transform infrared (FTIR) (Shimadzu FTIR-8400S Spectrum), which performed in the range of 4000 to 500 cm^{-1} at ambient temperature (25 ± 1 °C) using KBr pellets mixed at a ratio of 1 : 20, scanning electron microscopy (SEM) coupled with dispersive X-ray spectroscopy (EDX) (model JSM5910, Japan), Brunauer–Emmett–Teller (BET) analysis (Quantachrome-ASIQwin-USA), zeta potential (Nano Zs90) (Malvern, UK), X-ray diffraction (XRD) (JDX-3532, JEOL, Japan) (2θ range from 5 to 80°), and Raman analysis (InVia Raman microscope by RENISHAW UK).

2.2. Statistical analysis

The following resources were used to improve the efficacy and accuracy of current work: the Origin-Pro 2021 program was used to analyze the graphs. For a range of designing tasks and mathematical equations, Image-J and Math-Magic software (InfoLogics, version 3.61, 2022) were utilized. For XRD data processing, X'pert HighScore Plus (PANanalytical, version 3.0) was applied, whereas Endnote X9 (Clarivate, version 2021) was used for the reference style.

2.3. Materials/chemicals

Titanium tetra-isopropoxide ($C_{12}H_{28}O_4Ti$) (98%), P-nitrophenyl phosphate ($C_6H_6NO_6P$) (>99%), 2-methoxy ethanol ($C_3H_8O_2$) (>99.5%), sulphuric acid (H_2SO_4) (98%), and barium acetate ($C_4H_6BaO_4$) (>98.5%) were obtained from Sigma-Aldrich. Ethanol (99.7–100%), de-ionized water (DI), distilled water (DW) and, potassium chloride (KCl) (≥99.0%) were acquired from Riedel-deHaen. Phenol (C_6H_6O) (99.6%), Di-ethanol amine (DEA) (98%), potassium ferrocyanide ($C_6N_6FeK_4$) (98.5%), and potassium ferricyanide ($C_6N_6FeK_3$) (98%) were purchased from Daejung. Tenofovir hydrate drug (TFV) (98.0%), gemcitabine (GEM) (>99%), etoposide (ETO) (95–105%), ibuprofen (>98%), and diclofenac sodium (>98%) were bought from TCI. Alkaline phosphatase enzyme (ALP) was procured

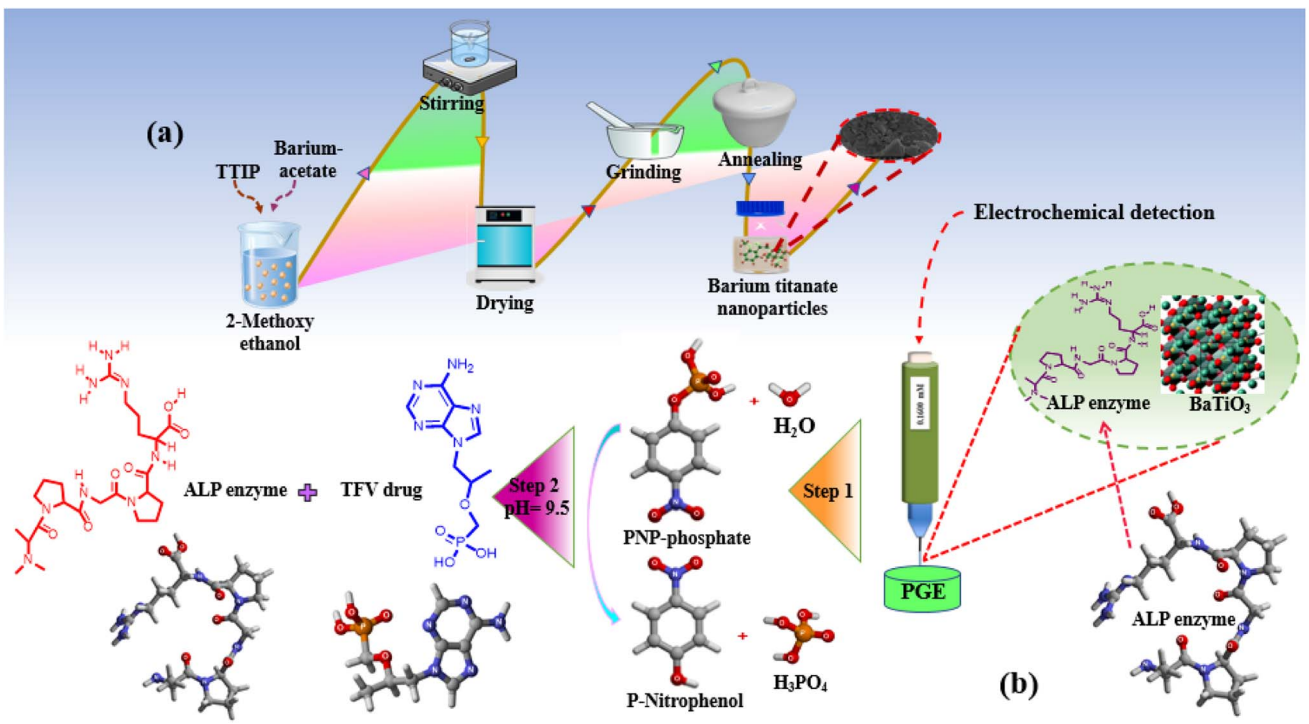

Scheme 1 (a) Synthesis of $BaTiO_3$ nanoparticles. (b) Modification of the electrode. (c) Possible mechanism for the detection of the TFV drug with 2D and 3D structures.

from Calbiochem, Human blood serum was obtained from a regional laboratory in Lahore. All chemicals and reagents used in this work were of analytical grade.

2.4. Synthesis of $BaTiO_3$

A well-known sol–gel method using economical starting materials was employed for the synthesis of $BaTiO_3$ nanopowders, as shown in Scheme 1a.[33] First, 50 mL of 2-methoxy ethanol was used to separately dissolve 5.476 g of barium acetate and 6.939 mL of titanium tetra-iso-propoxide over the course of 2 h. A barium titanate solution was prepared by mixing prepared solutions and stirring them consistently for an additional 2 h. The prepared solution was then dried inside a drying oven at 80 °C, and after thorough drying; the product was transferred to an electric furnace for further 2 h of annealing at 650 °C to form white-gray barium titanate crystals. These were then ground into fine powders. Using this method, $BaTiO_3$ nanoparticles were synthesized by following the proposed mechanism as shown in eqn (1)–(3). The first stage produces carbon dioxide gas when barium carbonate and 2-methoxyethanol mix to form barium 2-methoxyethoxide (1). The second stage involves a reaction between 2-methoxyethanol and titanium tetra-isopropoxide that produces titanium methoxyethoxide and isopropanol (2). In the last step, titanium methoxyethoxide and barium 2-methoxyethoxide react to produce barium titanate nanoparticles and methanol as a byproduct (3).

$$BaCO_3 + 2CH_3OCH_2CH_2OH \rightarrow Ba(OC_2H_4OCH_3)_2 + CO_2 \quad (1)$$

$$2CH_3OCH_2OH + Ti(OCH_2CH_3)_4 \rightarrow Ti(OCH_2CH_3) + 2C_3H_8O \quad (2)$$

$$Ba(OCH_3)_3 + Ti(OCH(CH_3)_2)_4 \rightarrow BaTiO_3 + 4CH_3OH \quad (3)$$

2.5. Preparation/pretreatment and electrochemical measurements of electrode fabrications

In the current research work, the PGE that had a diameter of approximately 0.50 mm and a length of 50 mm was used as a working electrode (WE). Before the modification of the PGE with nanoparticles, the surface was pretreated and cleaned electrochemically with 0.1 M sulfuric acid solution. Multiple cyclic voltammetry (CV) scans were conducted for this purpose, with potential ranges of −1.5 V to 1.0 V, in order to remove dust and other impurities.

To modify the electrode, an ultrasonicated grayish-white aqueous solution of 1 mg mL^{-1} of $BaTiO_3$ was used. The bare, cleaned electrode was immersed in 7.5 μL of the prepared $BaTiO_3$ solution for 45 min at room temperature. Once the electrode was totally dry, it was immersed in a 10 μL dilution of ALP enzyme for 15 min. After drying, the modified electrode was successfully used for electrochemical analysis using 20 μL of PNPP substrate in 2.5 mL of DEA buffer (pH = 9.50), using a 50 mV s^{-1} scan rate and a potential window of 0 V–1.4 V.

The electrode that was loaded with nanoparticles and enzymes was thoroughly dried before being submerged in a 10 μL solution of the TFV drug for 30 min to test the drug response. The modified electrode was dried before DPV scans in the same way as before. In the current investigation, all electrochemical measurements were carried out using a three-electrode system, consisting of an Ag/AgCl reference electrode, a platinum wire counter electrode, and a pencil graphite electrode (PGE) as the working electrode.

2.6. Optimization study

For the achievement of maximum sensitivity of the targeted analyte with the proposed sensor, several important experimental variables were evaluated. These variables included the effect of nanoparticles on enzyme activity, the impact of material concentration, the duration of electrode modification with nanoparticles, the incubation time for a given TFV drug concentration, and the modification time for the enzyme and materials.

2.7. Selectivity of the proposed sensor

Selectivity is an important parameter for developing an effective sensor, so in order to check the selectivity of the proposed sensor, the various potential interfering species such as gemcitabine (GEM), etoposide (ETO), ibuprofen (IBU) and diclofenac sodium (DIC) were examined under optimal conditions in the presence of a 20 μM TFV drug by using a DEA electrolyte and a PNPP substrate.

2.8. Preparation of real samples (blood serum)

Blood samples were collected and centrifuged for 10 min at 4000 rpm at room temperature. To reduce interferences during the experiment, serum samples were diluted ten times in a 0.1 M PBS solution (pH = 7.4, same as human blood) prior to analysis. The following concentrations of TFV were spiked into the diluted blood samples: 5 nM, 250 nM, and 3000 nM. The spiked serum samples were then subjected to DPV.

3. Results and discussion

3.1. UV analysis

The optical absorption spectra of $BaTiO_3$ nanoparticles at ambient temperature (25 °C) were obtained in the 200–800 nm wavelength range. The UV spectra displayed in Fig. 1a included a distinct absorbance peak at 235 nm in the UV region, which was in line with previously published data.[33] Based on the UV results, it was possible for Ba ions to be incorporated into the titania lattice during the synthesis of $BaTiO_3$ nanoparticles. This would increase the activity of photoelectrons and facilitate the electronic transition following photoexcitation. Consequently, while the targeted analyte is being sensed, its catalytic activity increases. Using Tauc's relation (4), the synthesized nanoparticles' direct band gap (E_g) was determined to be 3.5 eV.

$$(\alpha h\nu)^n = A(h\nu - E_g) \quad (4)$$

where "A" is a constant, "$h\nu$" is used to represent incident photon energy and "n" is the exponent (which may be 2 or 1/2) associated with the direct or indirect transition band gaps.

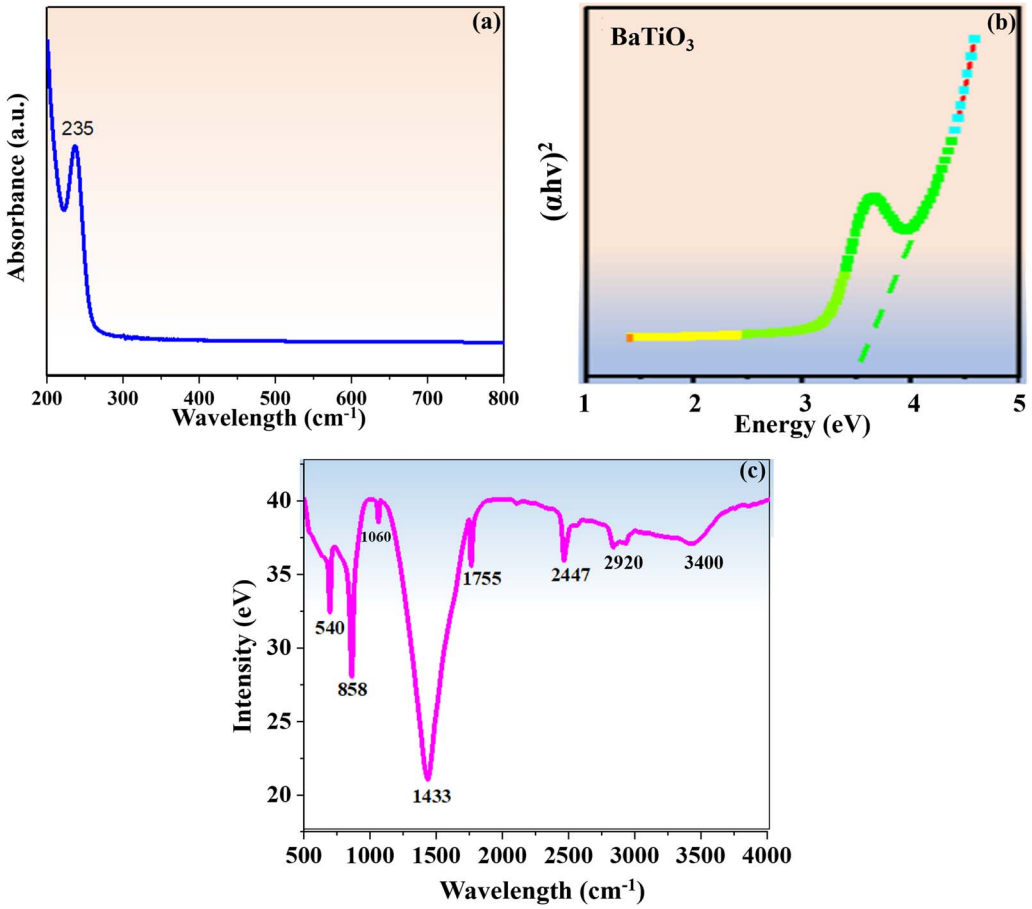

Fig. 1 (a) UV vis spectrum of $BaTiO_3$ nanoparticles. (b) Tauc's graph. (c) FT-IR spectrum of $BaTiO_3$ nanoparticles.

Tauc's graph for $BaTiO_3$ nanoparticles is shown in Fig. 1b. Because a nanomaterial's conductivity has a significant impact on band gap behavior, the synthesized nanosamples demonstrated remarkable conduction properties during electrochemical detection of the TFV drug in the subsequent study.

3.2. FT-IR analysis

The FT-IR spectra of the $BaTiO_3$ nanoparticles were recorded at ambient temperature (25 °C) in the wavenumber region of 4000–500 cm^{-1}, as shown in Fig. 1c The vibrational peaks at 540 cm^{-1}, 858 cm^{-1}, 1060 cm^{-1} and 1433 cm^{-1} indicated the stretching vibrations of the COO^-, Ba^-, $BaCO_3$, and Ti–OH bonds that were dominant in $BaTiO_3$ nanoparticles. These vibrations were highly supported by previous research.[34] The peaks at 2447 cm^{-1} and 3400 cm^{-1} show the stretching vibration of the –OH group that resulted from the presence of water molecules, while the peak at 1755 cm^{-1} represents the bending vibration of the COO– group brought on by the acetic acid ligand. The peak located at 2920 cm^{-1} signifies the appearance of the C–H functional group resulting from methoxy ethanol.

The carboxyl (–COOH) and amino ($-NH_2$) functional groups of ALP engage with the –OH group on nanoparticles, and this interaction plays a major role in the attachment of ALP to PGE *via* $BaTiO_3$ nanoparticles. The presence of numerous effective functional groups on $BaTiO_3$ nanoparticles creates a strong internal electric field, which greatly increased their catalytic effectiveness when TFV drug sensing was carried out using an ALP enzyme.

3.3. SEM and EDX analysis

The surface morphology and composition of the as-synthesized nanoparticles were analyzed by techniques of scanning electron microscopy (SEM) coupled with energy dispersive X-ray analysis (EDX). SEM micrographs of the $BaTiO_3$ nanoparticles (Fig. 2(a)–(c)) revealed the presence of spherical particles with hetrogeneous distribution along with a spatial arrangement of tiny grains.[35] The images show that the as-synthesized nanomaterials have a highly rough surface with cracks, pores, dislocations, or irregularities; this was important for the detection of the TFV drug because it provided strong support for the physical immobilization of ALP, which was further supported by the previously mentioned study.[36] $BaTiO_3$'s composition was further confirmed by EDX analysis, which demonstrated the presence of Ba, Ti, and oxygen atoms as seen in Fig. 2d. Furthermore, very little C-based contamination was found. Based on the results presented in Fig. 2e, the average calculated diameter of the $BaTiO_3$ nanoparticles was 20.764 nm, within the 5–40 nm range. The $BaTiO_3$ nanoparticles demonstrated excellent catalytic performance in detecting the TFV drug due to their small and ordered distribution pattern.

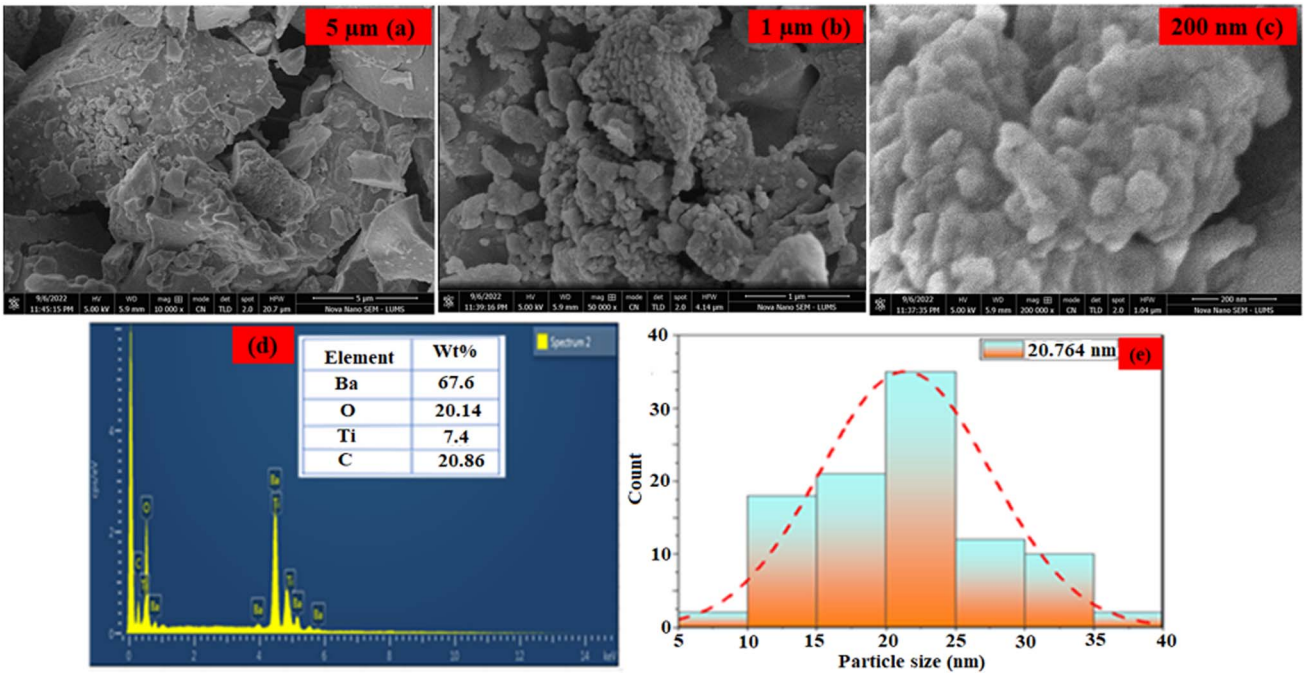

Fig. 2 (a–c) SEM image of $BaTiO_3$ nanoparticles. (d) EDX spectrum of $BaTiO_3$ nanoparticles. (e) particle distribution graph.

Under the BET analysis of N_2 adsorption/desorption measurements, the surface area and pore size of $BaTiO_3$ nanoparticles were determined. $BaTiO_3$ nanoparticles were estimated to have an average pore size of 2.1 nm and a surface area of 102.6 $m^2\ g^{-1}$. The synthesized nanoparticles' large surface area and small particle size significantly enhanced their catalytic activity in immobilizing biomolecules, as previously reported,[36] confirming their effectiveness in detecting the TFV drug.

3.4. Zeta potential analysis

The zeta potential of $BaTiO_3$ nanoparticles in water at a concentration of 2 mg mL^{-1} was measured using a DLS instrument. The He–Ne gas laser (633 nm) was used at a 90° scattering angle at ambient temperature. Zeta potential measurements on $BaTiO_3$ nanoparticles showed that they have a negative surface charge, measuring −0.922 mV. Because of the larger surface area and negative charge on nanoparticles, the ALP enzyme was able to bind and immobilize more easily. The literature reported that great stability could be demonstrated by nanomaterials with zeta potential values greater than +25 mV and less than −25 mV.[37]

After mixing the nanoparticles with ALP, the zeta potential indicated a strong interaction between them, with a value of −68.5 mV. A zeta potential of −979 mV was observed during testing a phenolic solution of $BaTiO_3$ nanoparticles, indicating high affinities of the nanoparticles for the substrate. The negative zeta potential of $BaTiO_3$ nanoparticles suggested the presence of surface charges that could interact with positively charged sites on ALP enzymes. In addition to electrostatic interactions, specific binding interactions between the enzyme and the surface of the $BaTiO_3$ nanoparticles, such as hydrogen bonds and hydrophobic interactions, also contributed to the observed immobilization. In addition to providing a stable platform for enzyme activity, immobilizing ALP on $BaTiO_3$ nanoparticles generated an efficient and sensitive biosensing environment for the TFV drug's detection.

3.5. XRD analysis

The X-ray diffraction pattern of the as-synthesized $BaTiO_3$ nanoparticles is shown in Fig. 3a. The study aligned with JCPDS no. 75-1539, indicating decisively that the synthesized $BaTiO_3$ nanoparticles matched well with previous studies as documented in the literature.[38] The crystalline structure of the perovskite nanoparticles was confirmed by XRD peaks at 2θ values of 20° (100), 23.95° (110), 43.05° (111), 46.95° (002), 47.88° (200), 58.98° (202), and 68.28° (300) The presence of $BaCO_3$, which came about as a result of a reaction between CO_2 and $BaTiO_3$ during annealing, was responsible for the other faint peaks visible in the sample's XRD spectrum.

Following Debye Scherer's eqn (5) from its sharpest peaks, the crystallite size for the as-synthesized nanoparticles was found to be 11 nm. The TFV drug's selective detection was shown to be greatly aided by the nanoparticles' well-crystalline structure and size. The ALP-modified electrode's stability, solidity, and dispersion were greatly enhanced by the crystalline nature of the nanoparticles, which in turn promoted the reaction.

$$D = K\lambda/\beta \cos\theta \quad (5)$$

where D indicates the particle size, K denotes Scherer's constant (0.98), λ represents the wavelength, and β is the full width half maximum.

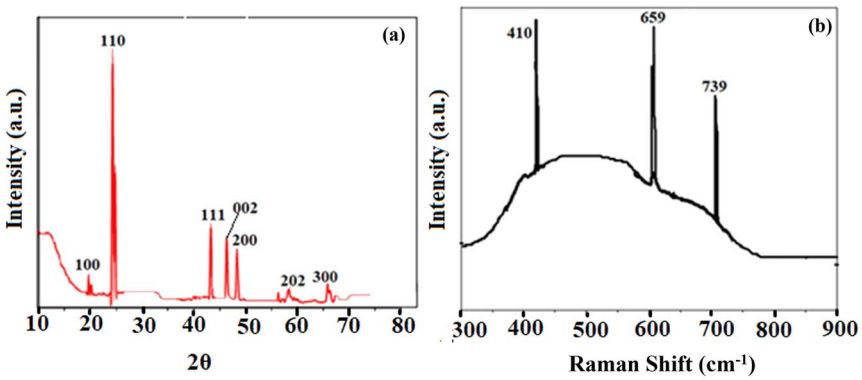

Fig. 3 (a) XRD pattern. (b) Raman spectra of $BaTiO_3$ nanoparticles.

3.6. Raman spectroscopic analysis

For studying structural deformation, Raman spectroscopy is a well-known, effective, and non-destructive technique. The Raman spectra of the $BaTiO_3$ nanoparticles that were produced were obtained within the spectral region of 300–900 cm^{-1}. Fig. 3b depicts the three Raman active modes of $BaTiO_3$, effectively showing its polycrystalline nature with various crystal orientations. The Raman shift of $BaTiO_3$ was reflected by the sharp peaks at 659 cm^{-1} and 739 cm^{-1}. On the other hand, the vibration due to the displacement of the oxygen atom in the TiO_6 group was responsible for the peak at 410 cm^{-1}. Numerous vibrational modes that were closely associated with the vibration of the crystal lattice were not detected at lower frequencies during the Raman analysis due to the tiny size of the applied materials.[39]

3.7. Electrochemical study

3.7.1. Electrochemical characterization. Important details on the electrochemical detection mechanism were acquired through the application of CV and electrochemical impedance spectroscopy (EIS). Ferro/ferricyanide plays a significant role in examining the redox couple behavior. In a 5 mM $(K_3Fe(CN)_6)$/$(K_4Fe(CN)_6)$ solution, the CVs of bare PGE, $BaTiO_3$/PGE, $BaTiO_3$/ALP/PGE, and $BaTiO_3$/ALP/TFV/PGE are displayed in Fig. 4A (scan rate 50 mV s^{-1} and potential range (−0.8 V–0.8 V)).

For a PGE, the peak currents for oxidation (*I*pa) and reduction (*I*pc) are 201.9 μA and 209.0 μA, respectively. With the electrode modified with $BaTiO_3$/PGE, the currents of *I*pa and *I*pc are reported to be 334.2 μA and 274.2 μA, respectively, leading to enhance conductivity and catalytic activity. The measured current values on $BaTiO_3$/ALP/PGE for *I*pa and *I*pc are 133.8 μA and 119.3 μA, respectively.

When compared to other electrodes, $BaTiO_3$/ALP/TFV/PGE displayed the lowest redox peaks, with *I*pa and *I*pc values of 111.1 μA and 111.6 μA, respectively. This could be the outcome of a possible interaction between the modified $BaTiO_3$/ALP electrode and the TFV drug. It is observed that the attachment of an additional drug to the modified electrode's surface reduced the electrode's electroactive surface area, which ultimately led to a decline in peak current. Randles–Sevcik eqn (6) was used to determine the active surfaces of these electrodes:

$$Ip = 2.69 \times 10^5 n^{3/2} AC\sqrt{Dv} \quad (6)$$

In this equation, *I*p stands for anodic peak current, *n* for the number of electrons transported, *A* for PGE surface area in cm^2, *C* for probe concentration, *D* for the diffusion coefficient in cm^2 s^{-1}, and *v* for sthe can rate in V s^{-1}. In terms of active surface area, the calculated values for a bare PGE, $BaTiO_3$/PGE, $BaTiO_3$/ALP/PGE, and $BaTiO_3$/ALP/TFV/PGE are 0.0121 cm^2, 0.0202 cm^2, 0.00826 cm^2, and 0.0068 cm^2 respectively. This result clearly

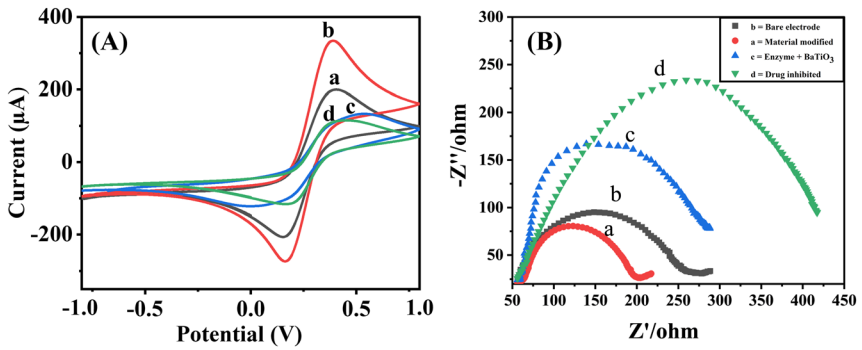

Fig. 4 (A) Cyclic voltammograms at scan rate 50 mV s^{-1} of (a) a bare PGE, (b) $BaTiO_3$/PGE, (c) ALP loaded $BaTiO_3$/PGE, and (d) TFV inhibited ALP loaded $BaTiO_3$/PGE. (B) The corresponding electrochemical impedance Nyquist plot.

supports that $BaTiO_3$/ALP considerably enhanced the active surface area of a PGE which is highly beneficial for the succeeding investigations the TFV drug.

EIS is yet another very efficient technique used to assess the electronic heterogeneity at the electrode interface. Therefore, it was used to further characterize the modified electrodes in a 5 mM $(K_3Fe(CN))_6/(K_4Fe(CN))_6$ solution. As shown in Fig. 4B, the Nyquist plot produced by EIS includes a semicircle component, with a smaller semicircle being detected for the surface of the bare electrode (b), indicating a lower charge transfer resistance (R_{ct}). The diameter of the semicircle significantly shrank when the bare electrode was modified with $BaTiO_3$ nanoparticles (a), indicating an improvement in the ability of $BaTiO_3$ nanoparticles to transfer charges. Additionally, for the ALP/$BaTiO_3$ electrode (c) and the TFV-modified ALP/$BaTiO_3$ electrode (d), the semicircle's diameter grew. The introduction of bioconjugation, which acts as a layer that hinders the transfer of electrons by redox probes from the electrode surface, caused fluctuations in the diameter of these semicircles,[18] and the subsequent CV results fully support the achieved EIS results.

3.7.2. Proof of concept against phenol. The CVs were conducted using 5 mM of phenol in a PBS solution (pH = 7.0) with bare and $BaTiO_3$-modified electrodes, confirming the nanoparticles' effectiveness against phenolic compounds using a potential window from 0 V to 1 V. The substantial physicochemical behavior of the electrode modified with nanoparticles led to a significant increase in its electrochemical activity towards the oxidation of phenol, as shown by the comparison study between the two functioning electrodes in Fig. 5a.

In fact, this idea offered a better platform for the integration of $BaTiO_3$ nanoparticles, as evident in subsequent investigations. The concept of the current study was further confirmed by using the UV-visible spectroscopic technique (wavelength ranged from 350 to 800 nm) in the presence of buffer solution of DEA (pH = 9.50) and a PNPP substrate. A mixture of an enzyme (ALP) (20 μL), TFV (10 μL), and buffer DEA (2.5 mL) was incubated for one hour prior to analysis. After this, 400 μL of PNPP was added, and a UV-visible spectrophotometer was used to analyze the mixture.

A significant quenching outcome was observed by the color change from colorless to yellowish in the spectra of the applied sample, as shown in Fig. 5b. The UV-visible spectrophotometric study revealed a decreased reaction (*i.e.*, less color change) as a result of TFV's capacity to inhibit the enzyme. This outcome evidently affirmed that the TFV drug was strongly attached to an ALP enzyme to significantly inhibit its activities.

3.7.3. Effect of nanoparticles on activity of the enzyme. It was feasible to evaluate the effect of nanoparticles on ALP enzyme activity by performing a CV scan in an electrolyte solution containing the PNPP substrate and DEA buffer (pH = 9.50). An electrode modified with ALP and $BaTiO_3$ nanoparticles showed a significantly better current response than an electrode treated with ALP alone, as shown in Fig. 6a. The use of low-cost $BaTiO_3$ nanoparticles, which significantly improved the immobilized ALP enzyme's sensing capabilities for the sensitive and selective detection of the intended analyte, is the primary innovation of the current study. The main advantages of using $BaTiO_3$ nanoparticles to support ALP are to increase its activity and protect it from denaturalization, which can be brought on by changes in the surrounding environment.

3.7.4. Effect of material concentration. $BaTiO_3$ nanoparticles played a catalytic role in enhancing the peak intensity during the analyte detection. The CV response (Fig. S1†) is significantly improved when $BaTiO_3$ nanoparticles are used as opposed to solely enzyme-modified electrodes, as demonstrated by Fig. 6a. The amount of $BaTiO_3$ nanoparticles on the surface of an electrode has a big impact on the electrode's electrochemical behavior. In order to obtain the best outcomes, $BaTiO_3$ solutions in the range of 5–15 μL were examined. DEA (pH = 9.50), an electrolyte buffer solution using PNPP, was subjected to the CV method. As shown in Fig. 6b, an increase in nanoparticle concentrations initially increased the current peak; however, after a certain point, a decrease in response was observed, most likely as a result of physical hindrance. Therefore, for obtaining maximum sensitivity, 7.5 μL of $BaTiO_3$ nanoparticle concentration was selected as an optimal modifier due to its excellent current response.

3.7.5. Electrode modification time with nanoparticles. To further investigate the performance of the $BaTiO_3$-modified electrode, the deposition time of the electrode with $BaTiO_3$ nanoparticles was studied for various time intervals (5–60 min). DPV analyses (Fig. S2(a)†)were performed in the potential range of 0 V–1.4 V using a PNPP substrate and an electrolyte buffer

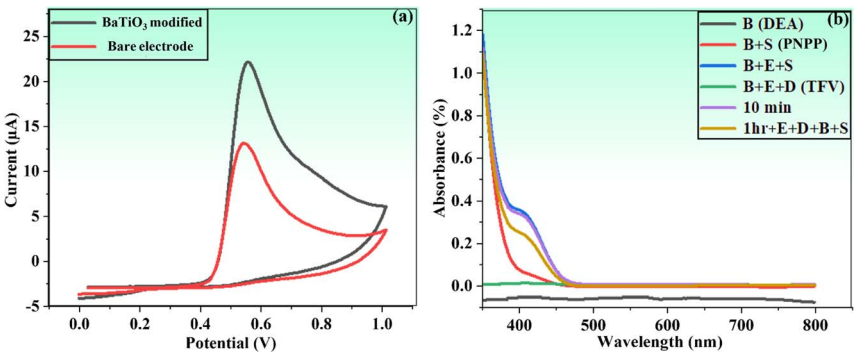

Fig. 5 (a) Cyclic voltammograms of bare PGE and $BaTiO_3$ nanoparticles modified against phenol in PBS. (b) UV/vis proof of concept of the proposed method.

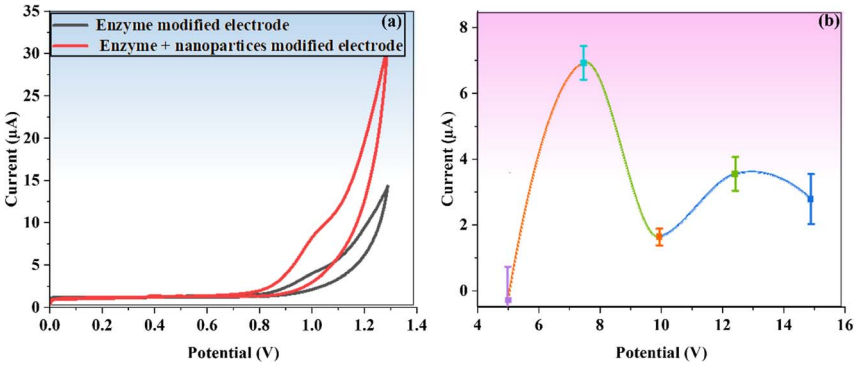

Fig. 6 Effect of nanoparticles on enzyme activity, (a) the enzyme loaded PGE (black line) and nanoparticle modified enzyme loaded PGE (red line). (b) Optimization of the nanoparticle amount to transform the PGE.

solution containing DEA (pH = 9.50). As seen in Fig. 7a, the current increased normally for 45 min before beginning to decrease due to an accumulation of nanoparticles that created a physical hindrance. Therefore, 45 min was found to be the optimal deposition time for $BaTiO_3$ nanoparticles due to its noteworthy contribution to later testing.

3.7.6. Modification time for a material with an enzyme. The effect of time on the modification of the electrode by $BaTiO_3$ and ALP ($BaTiO_3$/ALP) was investigated using DPV (Fig. S2(b)†) over a time range of 5–20 min, as illustrated in Fig. 7b. It is clear that, initially, the current value increased up to 15 min as the modification time increased, and then, as the binding sites on the electrode surface were saturated, a decreasing trend emerged. In light of this, 15 min was selected as the duration for a follow-up assessment of the oxidation of ALP products.

3.7.7. Incubation time for the same concentration of the TFV drug (200 nM). For the improved electrochemical detection of the TFV drug, its incubation time was investigated at various time periods (5–60 min) using the DPV technique. This was performed by dipping $BaTiO_3$/ALP/PGE in a 200 nM concentration of TFV drug in the buffer solution of DEA (pH = 9.50) and the PNPP substrate. The DPV analysis (Fig. S2(c)†) for the different time intervals displayed in Fig. 7c made it evident that the drug amount attachment increased over time, causing the rate of enzyme inhibition to progress. The optimal conditions led to the highest enzyme inhibition at 30 min, primarily due to the substantial drug attachment to the electrode surface. As

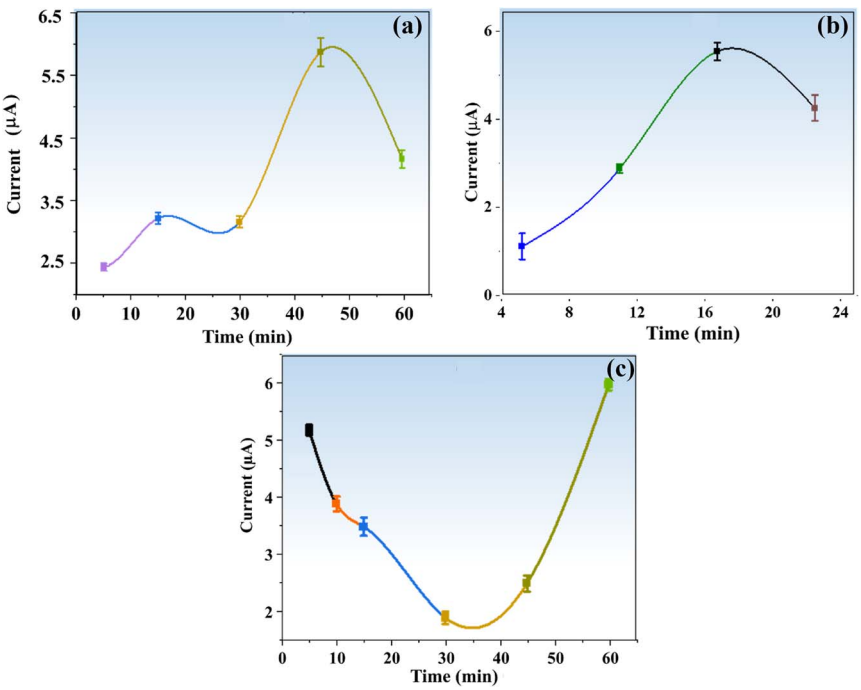

Fig. 7 (a) Electrode modification time with nanoparticles (b) electrode modification time with nanoparticles and enzymes. (c) Incubation time for the same concentration of the drug.

a result, 30 min time was chosen as the ideal deposition period and meticulously followed for subsequent tests.

3.8. Possible mechanism of action or the detection of TFV

The possible mechanistic study for the detection of the TFV drug is summarized in Scheme 1c. In an electrochemical ALP assay, the potential of $BaTiO_3$ nanoparticles for signal enhancement was clearly demonstrated. As a labeling enzyme, ALP is frequently used in electrochemical detection.[40,41] Along with ALP, PNPP was utilized as a substrate; however, its stability is much lower. Because high voltage is needed for electrochemical oxidation of the analyte, the primary drawback of using PNPP with an ALP-based electrochemical sensor is its limited sensitivity. A perovskite-based catalyst was employed to catalyze the reaction and accelerate oxidation in order to overcome this difficulty. The well-known perovskite nanostructure of $BaTiO_3$ has been used extensively to highlight its hidden performance in the field of sensing and actuators because of its extraordinary hole-conductive behavior (as high as σ = 100 S cm^{-1}).[42]

Owing to their surfaces' deficient sites and abundance of oxygen vacancies, the titanate family of perovskite materials is widely used to achieve promising catalytic activities in a variety of reactions.[43] $BaTiO_3$ nanoparticles have a wide range of uses in catalysis due to their strong structural stability and piezoelectric coefficient (d33) of 45 pC/N.[44,45] An additional driving force during the catalytic performance of $BaTiO_3$ nanoparticles was produced by the presence of an internal electric field, which greatly increased charge carrier mobility. Consequently, thermally stimulated carriers navigated the piezoelectric field without recombination. As a result, by permitting more piezoelectric-induced charge carriers to participate in the piezo–catalytic reaction,[46] during the sensing of the TFV drug by an ALP enzyme, this mechanism dramatically boosts the effectiveness of piezoelectric catalysis.

Adding $BaTiO_3$ to an analytical approach for TFV detection (Scheme 1c) resulted in a significant synergistic impact in the presence of both electrolytes and improved supporting properties for ALP. The TFV drug was detected using an enzymatic reaction based on ALP, which proved to be a dependable and sensitive transduction mechanism. An electrical signal was produced by the electroactive PNP, a well-known ALP dephosphorylation by-product of electrically inactive PNPP. By attaching more potential enzyme molecules to its surface, $BaTiO_3$ was able to increase enzymatic activity and amplify signals (PGE working electrode).

The synthesis of $BaTiO_3$ nanoparticles using the sol–gel method has the advantages of increased grain size and low inherent resistance, which significantly enhances sensing performance.[47] Therefore, for successful TFV detection, the special physicochemical properties of $BaTiO_3$ as a supporting material led to improved enzyme loading, stability, and catalytic activity.

The TFV drug was detected based on the ALP enzyme's dephosphorylation activity. In their respective structures, PNPP and TFV share phosphate groups with varying bond strengths. The current signal is produced by the ALP enzyme's assistance in converting PNPP into PNP, but the phosphate group of the TFV drug binds to the enzyme firmly, thus inhibiting it. An enzyme–substrate complex that forms during the detection process causes a decrease in the conversion of PNPP to PNP and, consequently, a drop in output current. The evaluation of the targeted analyte was based on this relative decrease in the electrical signal. Through optimization research, the best catalytic performance of ALP-$BaTiO_3$ was achieved in a DEA (2.5 mL) electrolyte solution (pH = 9.50). The DEA buffer was used to maintain a basic pH of 9.50, which is required for the ALP enzyme to function at its peak.

3.9. Detection of the TFV drug

To achieve higher sensitivity, TFV detection was thoroughly studied in pre-optimized settings with concentrations ranging from 1 to 3200 nM *via* DPV. Fig. 8a shows that when the concentration of the TFV drug increases, the oxidation peak current decreases correspondingly. With a correlation coefficient of $R^2 = 0.98759$, the relevant linear regression equation is *I*pa (nM) = 2.12436 (TFV nM) + (−3.41586), as seen in Fig. 8a. With a signal-to-noise ratio of 3 (S/N = 5), the calibration curve was used to determine the detection limit (LOD), which was found to be 0.09 nM.

The $BaTiO_3$/ALP/TFV/PGE sensor may be particularly effective at detecting the TFV drug, even at very low concentrations, as indicated by the lower value of acquired sensitivity. Furthermore, it can be compared well to some reported TFV bio(sensors) as given in Table 1, which implies that it is superior in terms of a lower LOD.

The enhanced conductivity and fast charge transfer at the modified electrode–electrolyte interface allowed the $BaTiO_3$/ALP/PGE biosensor to function exceptionally well in identifying the intended analyte. The number of active sites was enhanced by the modified electrode materials' synergistic impact, which significantly improved its electrochemical performance during detection. The goal of this strategy was to develop accurate and functional platforms for customized TFV drug detection by utilizing trustworthy tools. As a result, the investigation successfully verified the electrochemical technique for TFV drug quantitative detection at lower concentrations.

3.10. Detection of TFV drug by UV-visible spectrophotometry

The electrochemical detection of the TFV drug through the combination of $BaTiO_3$/ALP was further validated by the results of UV-visible spectrophotometry. Fig. 8b illustrates how the reaction time affects the absorbance shifting of the UV spectra throughout a wider range of TFV drug concentrations, from 1 to 3200 nM. When the ALP and substrate (20 μL) solution reached their maximum absorption at 1 nM, it was noted that their color changed from colorless to yellow, and up until 3200 nM, the color steadily declined. Fig. 8b shows the calibration plot for the UV-visible data ($R^2 = 0.921$). It was observed that at first, at a drug dose of 1 nM, there was less inhibition of enzyme activity, which resulted in a greater reaction, colored PNP and higher

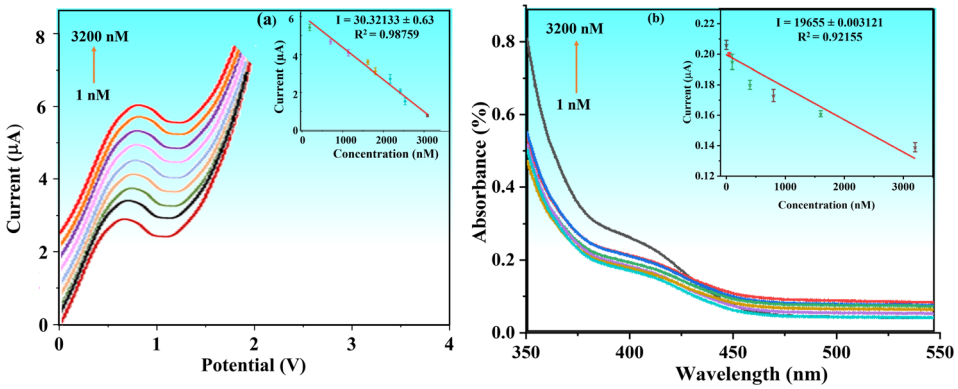

Fig. 8 (a) DPV and calibration plot of the TFV concentration response in the presence of various concentrations of TFV (1–3200 nM). (b) UV-vis absorbance by using different TFV concentrations (1–3200 nM).

Table 1 Comparison of different electrochemical sensors for the detection of the TFV drug

Sr.	Fabricated material	Limit of detection LOD (nM)	Ref.
1	MIP-Pt@g-C_3N_4/F-MWCNT	690	9
2	BDDE	560	48
3	La_2O_3–ZrO_2-MWCNTs	219	11
4	Cytochrome P450	1.2	40
5	Hg(Ag)FE	48.6	25
6	AgNP/BAC/GCE	239	41
7	ZrO_2-CS-MWCNTs	625	2
8	Adsorptive striping DPV/GCE	102.0	42
9	$BaTiO_3$/ALP/PGE	0.09	[Present work]

absorbance. The drug's concentration increased gradually, inhibiting the enzyme's available active sites on its surface. The majority of the active sites were blocked at 3200 nM of drug concentration, which resulted in lower activity and absorbance reduction.

3.11. Interference and reproducibility studies

To validate our methodology for selectively detecting the TFV drug amid potential interferences, we conducted a study. Establishing selectivity is crucial for sensor development and ensuring accurate TFV detection, which remains challenging in the presence of interfering species. We investigated several potential interferents, such as gemcitabine (GEM), etoposide (ETO), ibuprofen (IBU), and diclofenac sodium (DIC), using our optimized protocol. Fig. 9a demonstrates that the modified electrode had no detectable impact on the identified interfering species, even at high concentrations. These results confirm the exceptional selectivity and anti-interference performance of the suggested electrode (biosensor) for TFV detection in complex media like blood serum.

It is vital to evaluate analytical data reproducibility since it calls for extremely precise and exact measurement for practical applications.[49] Therefore, the reproducibility of $BaTiO_3$/ALP/TFV/PGE was scrutinized through the provision of five various electrodes in an electrolyte buffer solution of DEA at pH = 9.50 and a PNPP substrate, and DPV analysis was conducted in the presence of 400 nM TFV drug under the same experimental conditions (Fig. 9b). The calculated RSD value for the anodic current recorded by the seven electrodes for TFV was 4.9%, demonstrating the excellent reproducibility of the developed sensor.

3.12. Application of the methodology in a real medium (blood serum)

We applied the sensor for TFV detection in blood serum to assess its real-sample applicability. Blood serum is a complex medium with a wide range of proteins, peptides, hormones, enzymes,

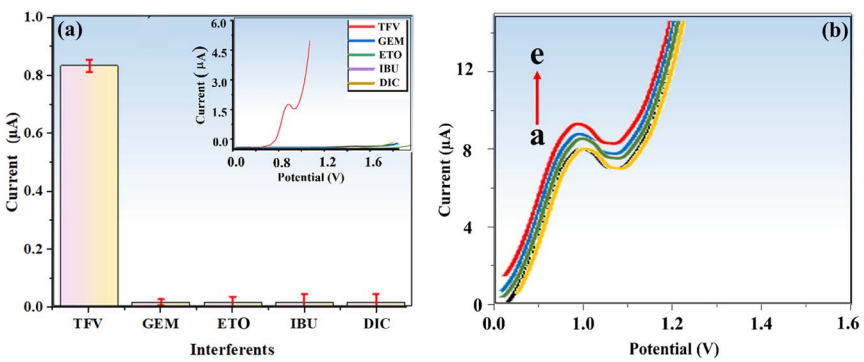

Fig. 9 (a) Interference studies with the number of drugs. (b) Electrode response reproducibility.

Table 2 Application of an electroactive $BaTiO_3$/ALP based biosensor in human blood serum and comparison with existing literature

This study				In the literature
Spiked (nM)	Found (nM)	R.S.D (%)	% Recovery	% Recovery material
5	5.3	4.119	106	95.14 (La_2O_3-(ZrO_2-WCNTs/GCE))[51]
250	246.6	0.968	98.6	98.0 (MIP-Pt@g-C_2N_4/F-MWCNT)[9]
3000	3085	1.930	102	97.87 (ZrO_2-CS-WCNTs/GCE)[52]

carbohydrates, lipids, amino acids, and small chemical molecules, making handling it challenging.[50] A standard addition method was used to spike the serum with various TFV drug concentrations. Table 2 displays the recovered percentages, which ranged from 98.6% to 106% for the proposed sensor as well as from some existing literature values. The efficacy of the $BaTiO_3$/ALP-based biosensor in real-time TFV drug monitoring was confirmed by these recovery measurements and compared well with that of the counterparts. Therefore, the suggested biosensor can be suitable for fabrication into a portable device for measuring small sample volumes and monitoring patients in need of immediate medical care and treatment.

4. Conclusion

In conclusion, this study has successfully developed a novel, simple, and relatively more efficient electrochemical biosensing platform for the specific and sensitive detection of the TFV drug. The platform is based on the ALP enzyme linked to the first reported signal modifier supported by $BaTiO_3$ nanoparticles. The synthesized nanoparticles were characterized and optimized under a variety of conditions, including the time of electrode modification with $BaTiO_3$ (45 min), incubation time for the same drug concentration (30 min), $BaTiO_3$ amount (7.5 μL), enzyme loading time on $BaTiO_3$/PGE (15 min), *etc.* The reported biosensor displayed an extremely low detection limit (LOD) of 0.09 nM in a linear dynamic range of 1–3200 nM. The proposed biosensor's potential for practical applications is supported by an interference or selectivity investigation conducted in the presence of numerous drug interferents. Additionally, this innovative method demonstrated an exceptional recovery percentage for the detection of the TFV drug in the samples of a highly complicated medium (human blood serum). The $BaTiO_3$/ALP biosensor is equipped with a reliable and cost-effective electrochemical sensing platform to be useful in point-of-care clinical analysis for the detection of TFV.

Author contributions

Muhammad Umar Draz and Muhammad Zia ul Haq: methodology, investigation, formal analysis, data curation, and writing – original article. Huma Ajab: supervision, analysis, software and review and editing. Akhtar Hayat: conceptualization, resources and validation.

Conflicts of interest

There are no conflicts to declare.

Acknowledgements

The Ministry of Science and Technology, Government of Pakistan, is acknowledged for a developmental grant titled "Establishment of Center for Advance Technologies in Biomedical Material" under its knowledge economy initiative.

References

1 R. Bawa, *Advances in Clinical Immunology, Medical Microbiology, COVID-19, and Big Data*, 2021.
2 J. Xiao, *et al.*, Fast and Ultrasensitive Electrochemical Detection for Antiviral Drug Tenofovir Disoproxil Fumarate in Biological Matrices, *Biosens*, 2022, **12**, 1123.
3 S. Ahmed, *et al.*, Assessment of hepatitis-related knowledge, attitudes, and practices on quality of life with the moderating role of internalized stigma among hepatitis B-positive patients in Pakistan, *Health Psychol. Behav. Med.*, 2023, **11**, 2192782.
4 J. R. Waymack and V. Sundareshan, *Acquired Immune Deficiency Syndrome*, 2019, p. 30725978.
5 A. A. Hyder and O. A. Khan, HIV/AIDS in Pakistan: the context and magnitude of an emerging threat, *J. Epidemiol. Commun. Health*, 1998, **52**, 579–585.
6 U. Waheed, *et al.*, Epidemiology of HIV/AIDS and Syphilis among high risk groups in Pakistan, *Pak. J. Zool.*, 2017, **49**, 1829–1834.
7 S. W. Teklu and T. T. Mekonnen, HIV/AIDS-pneumonia coinfection model with treatment at each infection stage: mathematical analysis and numerical simulation, *J. Appl. Math.*, 2021, **2021**, 1–21.
8 O. O. Apenteng, P. P. Osei, N. A. Ismail and A. Chiabai, Analysing the impact of migration on HIV/AIDS cases using epidemiological modelling to guide policy makers, *Infect. Dis. Model.*, 2022, **7**, 252–261.
9 M. Mehmandoust, M. Soylak and N. Erk, Innovative molecularly imprinted electrochemical sensor for the nanomolar detection of Tenofovir as an anti-HIV drug, *Talanta*, 2023, **253**, 12399.
10 S. Cavalera, *et al.*, Development and In-House Validation of an Enzyme-Linked Immunosorbent Assay and a Lateral Flow Immunoassay for the Dosage of Tenofovir in Human Saliva, *Biosens*, 2023, **13**, 667.
11 W. Zeng, *et al.*, Lanthanum doped zirconium oxide-nanocomposite as sensitive electrochemical platforms for Tenofovir detection, *Microchem. J.*, 2022, **183**, 108053.
12 S. Mohandoss, *et al.*, Tenofovir antiviral drug solubility enhancement with β-cyclodextrin inclusion complex and in

silico study of potential inhibitor against SARS-CoV-2 main protease (Mpro), *J. Mol. Liq.*, 2023, **377**, 121544.
13 J. Alake, *et al.*, Facile One-Step Synthesis of Nickel Sulphide Nanoparticles Decorated Poly (Acrylic Acid) Coated Multi-Walled Carbon Nanotube for Detection of Tenofovir in Human Urine, *Electrocatalysis*, 2023, **14**, 232–246.
14 S. O. Fakayode, *et al.*, Molecular (Raman, NIR, and FTIR) spectroscopy and multivariate analysis in consumable products analysis1, *Appl. Spectrosc. Rev.*, 2020, **55**, 647–723.
15 D. Xiao, *et al.*, An LC-MS/MS method for determination of tenofovir (TFV) in human plasma following tenofovir alafenamide (TAF) administration: development, validation, cross-validation, and use of formic acid as plasma TFV stabilizer, *Anal. Biochem.*, 2020, **593**, 113611.
16 T. S. K. Sharma and K. Y. Hwa, Facile Synthesis of Ag/$AgVO_3$/N-rGO Hybrid Nanocomposites for electrochemical detection of levofloxacin for complex biological samples using screen-printed carbon paste electrodes, *Inorg. Chem.*, 2021, **60**, 6585–6599.
17 A. Hayat and S. Andreescu, Nanoceria Particles As Catalytic Amplifiers for Alkaline Phosphatase Assays, *Anal. Chem.*, 2013, **85**, 10028–10032.
18 J. Hao, C. Li, K. Wu, C. Hu and N. Yang, Detection of tumor marker using ZnO@reduced graphene oxide decorated with alkaline phosphatase-labeled magnetic beads, *ACS Appl. Nano Mater.*, 2019, **2**, 7747–7754.
19 M. Awan, *et al.*, Fabrication of novel electroactive nickel sulfide@graphene oxide nanocomposite integrated transduction platform for non-enzymatic electrochemical sensing of Hydrogen Peroxide in environmental and biological samples, *Synth. Met.*, 2023, **292**, 117240.
20 K. Y. Goud, *et al.*, Electrochemical diagnostics of infectious viral diseases: trends and challenges, *Biosens. Bioelectron.*, 2021, **180**, 113112.
21 H. Teymourian, *et al.*, Wearable electrochemical sensors for the monitoring and screening of drugs, *ACS Sens.*, 2020, **5**, 2679–2700.
22 M. A. Khalilzadeh, S. Tajik, H. Beitollahi and R. A. Venditti, Green synthesis of magnetic nanocomposite with iron oxide deposited on cellulose nanocrystals with copper (Fe_3O_4@CNC/Cu): investigation of catalytic activity for the development of a venlafaxine electrochemical sensor, *Ind. Eng. Chem. Res.*, 2020, **59**, 4219–4228.
23 Z. Nate, A. A. Gill, R. Chauhan and R. Karpoormath, Polyaniline-cobalt oxide nanofibers for simultaneous electrochemical determination of antimalarial drugs: primaquine and proguanil, *Microchem. J.*, 2021, **160**, 105709.
24 F. A. Khan, Nanomaterials: types, classifications, and sources, *Applications of Nanomaterials in Human Health*, 2020, pp. 1–13.
25 N. Festinger, K. Spilarewicz-Stanek, K. Borowczyk, D. Guziejewski and S. Smarzewska, Highly sensitive determination of Tenofovir in pharmaceutical formulations and patients urine-Comparative electroanalytical studies using different sensing methods, *Molecules*, 2022, **27**, 1992.
26 G. Ozcelikay, B. Dogan-Topal and S. A. Ozkan, An Electrochemical Sensor Based on Silver Nanoparticles-Benzalkonium Chloride for the Voltammetric Determination of Antiviral Drug Tenofovir, *Electroanalysis*, 2018, **30**, 943–954.
27 A. Singh, R. K. Rawat and P. Chauhan, Design and development of SnO decorated $BaTiO_3$ heterostructure device platform for ethanol vapor detection, *J. Mater. Sci.: Mater. Electron.*, 2022, **33**, 18220–18230.
28 S. Selvarajan, N. R. Alluri, A. Chandrasekhar and S. J. Kim, Direct detection of cysteine using functionalized $BaTiO_3$ nanoparticles film based self-powered biosensor, *Biosens. Bioelectron.*, 2017, **91**, 203–210.
29 E. Pourtaheri, M. A. Taher and H. Beitollahi, Synergistic Signal Amplification Based on Ionic Liquid-$BaTiO_3$ Nanoparticle Carbon Paste Electrode for Sensitive Voltammetric Determination of Acetaminophen, *Anal. Bioanal. Chem. Res.*, 2018, **5**, 261–271.
30 H. Jiao, *et al.*, Barium titanate (1 0 1)/silver nanocomposite: preparation, photocatalytic activity, and mechanism based on Density Functional Theory, *Mater. Sci. Eng. B*, 2023, **288**, 116137.
31 S. Selvarajan, N. R. Alluri, A. Chandrasekhar and S. J. Kim, $BaTiO_3$ nanoparticles as biomaterial film for self-powered glucose sensor application, *Sens. Actuators, B*, 2016, **234**, 395–403.
32 S. Gianvittorio, I. Gualandi and D. Tonelli, ALP-Based Biosensors Employing Electrodes Modified with Carbon Nanomaterials for Pesticides Detection, *Molecules*, 2023, **28**, 1532.
33 M. Singh, B. C. Yadav, A. Ranjan, M. Kaur and S. K. Gupta, Synthesis and characterization of perovskite barium titanate thin film and its application as LPG sensor, *Sens. Actuators, B*, 2017, **241**, 1170–1178.
34 O. Harizanov, A. Harizanova and T. Ivanova, Formation and characterization of sol-gel barium titanate, *Mater. Sci. Eng., B*, 2004, **106**, 191–195.
35 S. Sagadevan and J. Podder, Investigation of structural, SEM, TEM and dielectric properties of $BaTiO_3$ nanoparticles, *J. Nano- Electron. Phys.*, 2015, **7**, 04008.
36 H. Hayashi, T. Nakamura and T. Ebina, In-situ Raman spectroscopy of $BaTiO_3$ particles for tetragonal–cubic transformation, *J. Phys. Chem. Solids*, 2013, **74**, 957–962.
37 M. Buzdar, *et al.*, Paper based colorimetric sensor using novel green magnetized nanocomposite of pinus for hydrogen peroxide detection in water and milk, *Food Biosci.*, 2023, **55**, 103014.
38 M. Biglar, F. Stachowicz, T. Trzepieciński and M. Gromada, Synthesis of barium titanate piezoelectric ceramics for multilayer actuators (mlas), *Acta Mech.*, 2017, **11**, 766.
39 M. Yoshikawa, M. Murakami and H. Ishida, Highly sensitive detection of near-field Raman scattered light from strained Si/SiGe heterostructures by scanning near-field optical Raman microscope using ultraviolet resonant Raman scattering, *Appl. Phys. Lett.*, 2008, **92**, 091903.
40 N. Aliakbarinodehi, *et al.*, Aptamer-based field-effect biosensor for tenofovir detection, *Sci. Rep.*, 2017, **7**, 44409.

41 G. Ozcelikay, B. Dogan-Topal and S. A. Ozkan, An electrochemical sensor based on silver nanoparticles-benzalkonium chloride for the voltammetric determination of antiviral drug tenofovir, *Electroanalysis*, 2018, **30**, 943–954.
42 G. Ozcelikay, B. Dogan-Topal and S. A. Ozkan, Electrochemical characteristics of tenofovir and its determination in dosage form by electroanalytical methods, *Rev. Roum. Chim.*, 2017, **62**, 569–578.
43 N. A. Spaldin, S. W. Cheong and R. Ramesh, Multiferroics: past, present, and future, *Phys. Today*, 2010, **63**, 38–43.
44 Z. Wang, J. Hu, A. P. Suryavanshi, K. Yum and M. F. Yu, Voltage Generation from Individual $BaTiO_3$ Nanowires under Periodic Tensile Mechanical Load, *Nano Lett.*, 2007, **7**, 2966–2969.
45 Z. Y. Shen and J. F. Li, Enhancement of piezoelectric constant d33 in $BaTiO_3$ ceramics due to nano-domain structure, *J. Ceram. Soc. Jpn.*, 2010, **118**, 940–943.
46 S. Kappadan, T. W. Gebreab, S. Thomas and N. Kalarikkal, Tetragonal $BaTiO_3$ nanoparticles: an efficient photocatalyst for the degradation of organic pollutants, *Mater. Sci. Semicond. Process.*, 2016, **51**, 42–47.
47 M. Shellaiah and K. W. Sun, Review on sensing applications of perovskite nanomaterials, *Chemosensors*, 2020, **8**, 55.
48 K. Morawska, T. Popławski, W. Ciesielski and S. Smarzewska, Electrochemical and spectroscopic studies of the interaction of antiviral drug Tenofovir with single and double stranded DNA, *Bioelectrochemistry*, 2018, **123**, 227–232.
49 H. Ajab, A. Yaqub, M. S. Nazir, M. Z. H. Rozaini and M. A. Abdullah, Optimization of oil palm-based cellulose and hydroxyapatite-carbon composite electrode for trace Pb (II) ions detection in aqueous system, *Bioresour*, 2020, **15**, 6273–6281.
50 R. S. Tirumalai, *et al.*, Characterization of the Low Molecular Weight Human Serum Proteomes, *Mol. Cell. Proteomics*, 2003, **2**, 1096–1103.
51 W. Zeng, *et al.*, Lanthanum doped zirconium oxide-nanocomposite as sensitive electrochemical platforms for Tenofovir detection, *Microchem. J.*, 2022, **183**, 108053.
52 J. Xiao, *et al.*, Fast and Ultrasensitive Electrochemical Detection for Antiviral Drug Tenofovir Disoproxil Fumarate in Biological Matrices, *Biosensors*, 2022, **12**(12), 1123.